THE EUROPEAN PHYSICAL JOURNAL PLUS

Accepted 17 November 2021

www.springer.com/journal/13360

Impact factor = 3.911

Heat transfer and entropy generation analysis of water-Fe_3O_4/CNT hybrid magnetic nanofluid flow in a trapezoidal wavy enclosure containing porous media with the Galerkin finite element method

Weal Al-Kouz[1], Aissa Abderrahmane[2], MD. Shamshuddin[3], Obai Younis[4,5], Sahnoun Mohammed[2], O. Anwar Bég[6], Davood Toghraie[7,a]

[1] Mechanical and Maintenance Engineering Department, School of Applied Technical Sciences, German Jordanian University, Amman 11180, Jordan.

[2] Laboratoire de Physique Quantique de la Matière et Modélisation Mathématique (LPQ3M), Université Mustapha Stambouli de Mascara, Mascara, Algeria.

[3] Department of Mathematics, Vaagdevi College of Engineering (Autonomous), Warangal, Telangana, India.

[4] College of Engineering at Wadi Addwaser, Mechanical Engineering Department, Prince Sattam Bin Abdulaziz University, Wadi Addwaser, Saudi Arabia.

[5] Department of Mechanical Engineering, Faculty of Engineering, University of Khartoum, Khartoum, Sudan

[6] Professor of Mechanical Engineering Science, MPESG, Mechanical Engineering Dept. School of Science, Engineering and Environment (SEE), University of Salford, Manchester M54WT, UK

[7] Department of Mechanical Engineering, Islamic Azad University, Khomeinishahr, Iran.

Abstract:

The present study addresses theoretically and computationally the performance of electrically conducting water-Fe_3O_4/CNT hybrid nanofluid in three-dimensional natural convective heat transfer and entropy generation within a wavy-walled trapezoidal enclosure. The enclosure has two layers - a hybrid nanofluid layer and a porous medium layer. A transverse magnetic field is applied in the upward direction. Newtonian flow is considered and the modified Navier-Stokes equations are employed with Lorentz hydromagnetic body force, Darcian and Forchheimer drag force terms. The wavy side planes are heated down while the top and vertical planes are thermally insulated. A rectangular heated fin is placed in the lower plane and several different locations of the fin are considered. The transformed, non-dimensional system of coupled non-linear partial differential equations with associated boundary conditions is solved numerically with the Galerkin finite element method (FEM) in the COMSOL Multiphysics software platform. The effects of Darcy number, Hartmann number, volume fraction, undulation number of the wavy wall and Rayleigh number (thermal buoyancy parameter) on the streamlines, isotherms and Bejan number contours are studied. Extensive visualization of the thermal flow characteristics is included. With increasing Hartmann number and Rayleigh number, the average Bejan number is reduced strongly whereas average Nusselt number is only depleted significantly at very high Rayleigh number and high Hartmann number. With increasing undulation number, there is a slight elevation in average Bejan number at intermediate Rayleigh numbers, whereas the average

Nusselt number is substantially boosted, and the effect is maximized at very high Rayleigh number. Increment in Darcy number (i. e. reduction in permeability of the porous medium layer) is observed to considerably elevate average Nusselt number at high values of Rayleigh number, whereas the contrary response is computed in average Bejan number. The simulations are relevant to hybrid magnetic nanofluid fuel cells and electromagnetic nano-materials processing in cavities.

Keywords: *Entropy generation, Darcy-Forchheimer model, Porous media; CNT, Hybrid nanofluid, Nanoparticles, Galerkin Finite-Element method, COMSOL Multiphysics software.*

1. Introduction

Conventional thermal fluids such as ethylene glycol (EG), oil and water continue to play critical roles in a wide range of technological applications, particularly in power production and heating/cooling systems. Their heat transfer capability, however, is limited by their inadequate thermal conductivity. Nanofluids are fluids prepared by the dispersing of metallic or non-metallic nanoparticles in base fluids. The addition of these dispersed particles to conventional fluids improves the thermal conductivity of the host fluid [1–3]. Owing to their potential heat transfer improvements, nanofluids have been the topic of extensive research in recent years [4-9]. Nanofluids have the versatility to contribute to a variety of practical technologies such as thermal power, transportation, electronic cooling, biomedical systems, and renewable energy devices. Nowadays, many studies on the thermal conductivity improvement capabilities of metallic and oxide nanoparticles, carbon nanofibers and carbon nanotubes within conventional fluids (e. g. water, ethylene glycol) have been published. Numerous methods for enhancing the thermal conductivity and heat transfer characteristics of nanofluids have therefore been developed around the world [10–16]. These reported studies on theoretical and experimental investigations have revealed that the thermal conductivity of nanofluids is affected by a variety of parameters, including particle volume fraction, particle material, particle size, particle shape, base fluid, and temperature. It has also been demonstrated that the amount and type of additives, as well as the acidity of the nanofluid, may improve thermal conductivity [17-18].

While continuing to study nanofluids, researchers have recently attempted to implement *hybrid nanofluids* which are synthesized by suspending combinations of various nanoparticles in mixtures or composite materials. The idea of using hybrid nanofluids is to synergistically balance the properties of their constituent materials to create elevate thermal conductivity more effectively than *unitary* (i. e. single nanomaterial-doped) nanofluids. The new generation of hybrid nanomaterials are mainly composed of carbon nanotubes and metals, semiconductors or composites of non-conductive nanoparticles and carbon nanotubes. Salman *et al.* [19] conducted an extensive review of numerous studies on improving heat transfer with and without hybrid nanofluids. Their study showed an increase in heat transfer using a hybrid

nanofluid as the working fluid and also an improvement in the heat transfer coefficient as the nanoparticle volume and concentration of the hybrid nanofluid increased. Suresh *et al*. [20] experimentally investigated the effect of Al_2O_3-Cu/water hybrid nanofluids on convective heat transfer, observing the greatest improvement of 13.56% in Nusselt number at Reynolds number of 1730 compared to the pure water Nusselt number. They also demonstrated that 0.1% Al_2O_3--Cu/water hybrid nanofluid has a slightly higher coefficient of friction compared with the 0.1% Al_2O_3-/water nanofluid. Shahsavar *et al.* [21] studied numerically the heat transfer and entropy generation properties of water-based hybrid nanofluids (Fe_3O_4 (magnetite) nanoparticles and carbon nanotubes (CNTs) in water) in natural convection flow within a concentric horizontal ring. They noted that increasing the Fe_3O_4 and CNT concentrations (for a constant Rayleigh number) leads to an increase in the rate of entropy generation. Labib *et al.* [22] have also numerically investigated the effect of base fluids and hybrid nanofluid (mixture of Al_2O_3 nanoparticles and carbon nanotubes (CNTs) suspended in water) in forced convective heat transfer, noting significant improvement in thermal performance with. They also observed that CNT-nanofluid exhibit higher shear thinning behavior compared with hybrid nanofluid.

The above studies have shown that computational modelling provides a very useful compliment to experimental studies. In order to enable different test situations to be compared, before making any experimental prototype of a unitary or hybrid nanofluid, numerical simulation has emerged as a powerful and comparatively less expensive approach. Many different geometrical configurations are of interest for internal flow applications of nanofluids including annular (tubes), cubic enclosures, trapezoidal, spherical etc. These designs feature frequently in solar energy and materials processing technologies in which natural convection phenomena arise frequently. A further geometry is the wavy enclosure (cavity with undulating boundary) which has been deployed extensively in renewable power generation, thermal insulation, industrial cooling systems, lubrication systems, solar energy panels, biol-fuel cells, underground cable systems, and electric equipment [23]. Ali *et al.* [24] investigated numerically the flow and heat transfer components of buoyancy driven convection in a hybrid nanofluid filled wavy-walled enclosure containing obstacles, showing that the strength of fluid motion is intensified for a wavy cavity containing heat generating obstacle compared to smooth cavity without blockage. Maximum heat transfer is ensured at lower heater length and radius of the heat generating cylinder. Heat transfer rate also increases with the roughness of the cavity. Azizul *et al*. [25] examined numerically the mixed convection of nanofluids in an enclosure featuring of a heat source at the base and a cold top wavy surface. They used a Galerkin finite element technique to compute velocity and the temperature characteristics,

noting that larger values of the Richardson number and the Reynolds number enhance the rate of heat transfer. They also simulated the effects of different numbers of undulations and locations of the heat source. Ishak *et al*. [26] simulated numerically using a finite element technique, the entropy production in mixed convection within a trapezoidal nanofluid-filled enclosure containing a localized solid cylinder. In this study, it was reported that the solid cylinder radius and location are significant control parameters for optimizing the heat transfer inside the trapezoidal cavity. Furthermore, the maximum average Nusselt numbers are obtained for high cylinder radius values, where the average Nusselt number is increased by 30% with an increase in cylinder radius to 0.25. Ahmed and Rashed [27] carried out numerical simulation of magnetohydrodynamic free convection and heat transfer of nanofluids flow inside wavy enclosures filled with a heat generating porous medium, under effects of an inclined magnetic field with constant strength and a source of a heat generation within a constant volumetric rate. It was observed that the wall waviness influences the heat transfer rate and the flow regime structure significantly.

To the best knowledge of the authors, thus far no archival publications have considered the detailed behavior of the natural convective heat transfer and entropy generation in magnetohydrodynamic hybrid nanofluid flow in wavy-walled enclosures. In this paper, the problem of three-dimensional natural convection of water/Fe_3O_4 and MWCNT's hybrid nanofluid in trapezoidal enclosures having wavy planes is addressed theoretically and computationally using COMSOL software (Galerkin finite element method). Separate layers in the enclosure are studied- namely a nanofluid layer and a porous medium layer with the Darcy-Forchheimer drag force model. The side wavy planes are heated down while the top and vertical planes are thermally insulated. A rectangular heated fin is placed in the lower plane and several cases based on the location of the fin are considered. Furthermore, a constant magnetic field is taken in the normal direction (z-direction) while gravity is considered in the negative *z*-direction. The effects of nanoparticles volume concentration and Rayleigh number on the streamlines, isotherms, average Nusselt number and the local and global thermal entropy generation rate, frictional entropy generation rate and total entropy generation rate are analyzed and visualized graphically. Extensive interpretation of the results is included. The simulations are relevant to hybrid wavy nanofluid fuel cells [28-30] and magnetic nanofluid fuel cell design [31, 32] in which the combination of wavy boundaries and nanofluids have been shown to provide enhanced thermal performance.

2. Mathematical model

The regime under consideration in a Cartesian coordinate system (x, y, z) examines steady, three-dimensional, laminar natural convection flow in a trapezoidal enclosure under a transverse magnetic field applied in the negative x-direction. Density of the electrically conducting nanofluid is constant i. e. incompressible flow is studied. **Figure 1** show the physical model of the problem which comprises 3D trapezoidal enclosures with wavy side base planes. To formulate the mathematical model governing the convective transport, the following assumptions are taken into account:

- The side wavy planes are heated down while the top and vertical planes are thermally insulated.
- A rectangular heated fin is placed in the *lower* plane and several cases based on the location of the fin are considered.
- A constant magnetic field is imposed along the reverse x-direction while the gravity acts in the downward direction.
- The domain of flow is divided to multi-layers, namely, a hybrid nanofluid layer and a porous medium layer. Dilute nanofluids are considered via a modified Tiwari-Das model.
- Hybrid nanofluid is considered i. e. water as base fluid with Fe_3O_4 and MWCNT's nanoparticles.
- The one-energy equation model (thermal equilibrium state) is applied during the formulation of the problem and the mixture density is a linear function of the temperature.

The wavy walls equations obey the following geometric relation:

$$x = -A\sin\left(\frac{N\pi x}{H}\right) \tag{1}$$

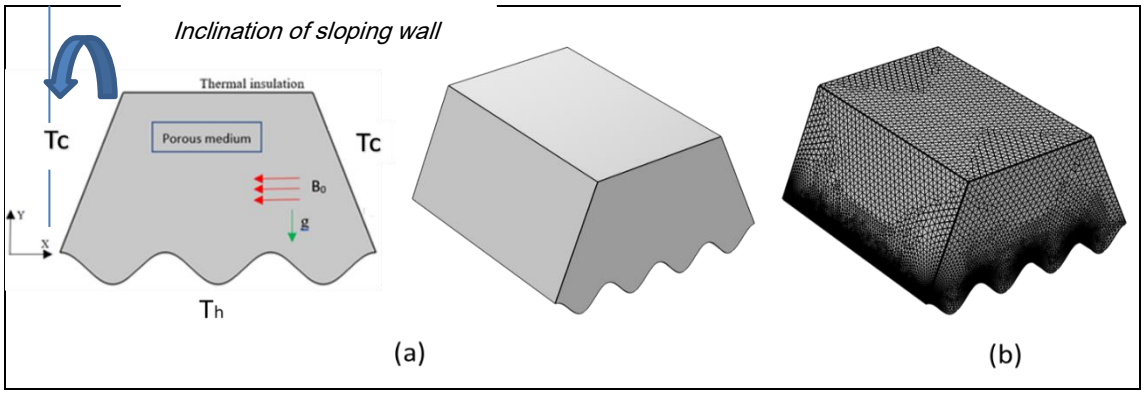

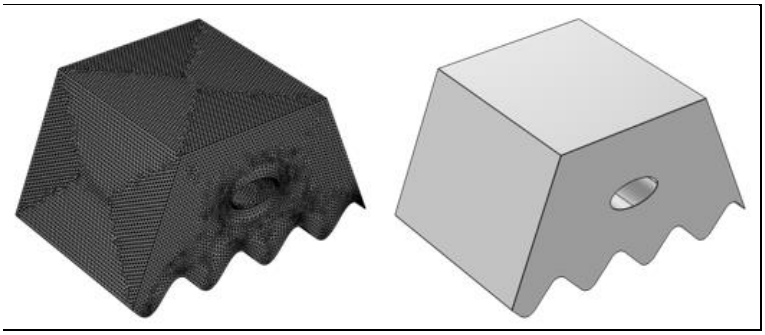

(c)

Fig 1. (a) Geometry in 2 D (side elevation) (b) 3D view of trapezoidal enclosure model with associated mesh. (b) 3-D view of finned wall with mesh.

By considering all the afore-mentioned assumptions, the appropriate conservation equations are:

Porous Layer:

$$\nabla \cdot \mathbf{v} = 0, \tag{2}$$

$$\frac{\rho_{hnf}}{\varepsilon^2} v \cdot \nabla v = -\nabla p + \nabla \cdot \left(\frac{\mu_{hnf}}{\varepsilon} \nabla v\right) - \frac{\mu_{hnf}}{K} v - \frac{C_F}{\sqrt{K}} |v| v - (\rho\beta)_{hnf}(T - T_c)\vec{g} + \frac{\sigma_{hnf}}{\varepsilon} \boldsymbol{v} \times \vec{\boldsymbol{B}}, \tag{3}$$

$$\left(\rho C_p\right)_{hnf} \mathbf{v} \cdot \nabla T = \nabla \cdot \left(k_m \nabla T\right), \tag{4}$$

Where C_F is the inertia (Forchheimer) coefficient of the porous medium, $C_F = 1.75 / \left(\sqrt{150}.\varepsilon^{1.5}\right)$ [33], ε is the porosity of the medium, K is the permeability of the porous medium that is described as the following: k_m is the effective thermal conductivity of the porous medium, $k_m = (1-\varepsilon)k_s + \varepsilon k_{hnf}$ where k_s and k_{hnf} are the thermal conductivities of the solid framework and fluid, respectively. υ_m is the effective kinetic viscosity of a porous medium, H is enclosure height**,** $\boldsymbol{v}$ is the velocity vector, $\vec{\boldsymbol{B}}$, is magnetic field vector, ρ is density, T is temperature and σ_{hnf} is the electrical conductivity of the magnetic nanofluid, N is undulation number of the wavy wall, A is amplitude of the waviness. To facilitate numerical solutions, it is judicious to invoke the following non-dimensional parameters:

$$\begin{gathered}(X,Y) = \frac{x,y}{L},\ (U,V,W) = \frac{(u,v,w)L}{\alpha_{nf}}, \theta = \frac{T - T_c}{T_h - T_c}, P = \frac{(p)}{\rho_{nf}\frac{\alpha_{fl}^2}{L^2}}, \\ Ra = \frac{g\beta_{fluid}(T_h - T_c)L^3}{\alpha_{fluid}\nu_{fluid}}, Da = \frac{K}{L^2},\ \Pr = \frac{\nu_{fluid}}{\alpha_{fluid}},\ Ha = LB\sqrt{\frac{\sigma_{nf}}{\mu_{nf}}}\end{gathered} \tag{5}$$

Here X, Y are dimensionless coordinates, U, V,W are the dimensionless velocity components, θ is dimensionless temperature, P is dimensionless pressure, Ra is Rayleigh number (thermal buoyancy or natural convection parameter), Da is Darcy number (dimensionless permeability), Pr is Prandtl number and Ha is the Hartmann number (ratio of Lorentzian magnetic body force to viscous hydrodynamic force) and L is length of the enclosure.

The previous two systems are combined in one system which in dimensionless form is expressed as follows:

Continuity:

$$\frac{\partial U}{\partial X}+\frac{\partial \mathrm{V}}{\partial Y}+\frac{\partial W}{\partial Z}=0, \tag{6}$$

Momentum:

$$\begin{aligned}\frac{1}{\varepsilon^2}\frac{\rho_{hnf}}{\rho_{fluid}}\left(U\frac{\partial U}{\partial X}+V\frac{\partial U}{\partial Y}+W\frac{\partial U}{\partial Z}\right)=&-\frac{\partial P}{\partial X}+\frac{1}{\varepsilon}\frac{\upsilon_{hnf}}{\upsilon_{fluid}}\mathrm{Pr}\left(\frac{\partial^2 U}{\partial X^2}+\frac{\partial^2 U}{\partial Y^2}+\frac{\partial^2 U}{\partial Z^2}\right)\\&-\frac{\upsilon_{hnf}}{\upsilon_{fluid}}\frac{\mathrm{Pr}}{Da}U-\frac{F_c}{\sqrt{Da}}U\sqrt{U^2+V^2+W^2}\\&-\frac{\sigma_{hnf}}{\sigma_{fluid}}\frac{\mathrm{Pr}\,Ha^2}{\varepsilon}U,\end{aligned} \tag{7}$$

$$\begin{aligned}\frac{1}{\varepsilon^2}\frac{\rho_{hnf}}{\rho_{fluid}}\left(U\frac{\partial V}{\partial X}+V\frac{\partial V}{\partial Y}+W\frac{\partial V}{\partial Z}\right)=&-\frac{\partial P}{\partial Y}+\frac{1}{\varepsilon}\frac{\upsilon_{hnf}}{\upsilon_{fluid}}\mathrm{Pr}\left(\frac{\partial^2 V}{\partial X^2}+\frac{\partial^2 V}{\partial Y^2}+\frac{\partial^2 V}{\partial Z^2}\right)\\&-\frac{\upsilon_{hnf}}{\upsilon_{fluid}}\frac{\mathrm{Pr}}{Da}V-\frac{F_c}{\sqrt{Da}}V\sqrt{U^2+V^2+W^2}\\&-\frac{\sigma_{hnf}}{\sigma_{fluid}}\frac{\mathrm{Pr}\,Ha^2}{\varepsilon}V,\end{aligned} \tag{8}$$

$$\begin{aligned}\frac{1}{\varepsilon^2}\frac{\rho_{hnf}}{\rho_{fluid}}\left(U\frac{\partial W}{\partial X}+V\frac{\partial W}{\partial Y}+W\frac{\partial W}{\partial Z}\right)=&-\frac{\partial P}{\partial Z}+\frac{1}{\varepsilon}\frac{\upsilon_{hnf}}{\upsilon_{fluid}}\mathrm{Pr}\left(\frac{\partial^2 W}{\partial X^2}+\frac{\partial^2 W}{\partial Y^2}+\frac{\partial^2 W}{\partial Z^2}\right)\\&-\frac{\upsilon_{hnf}}{\upsilon_{fluid}}\frac{\mathrm{Pr}}{Da}W-\frac{F_c}{\sqrt{Da}}W\sqrt{U^2+V^2+W^2}\\&+\frac{\beta_{hnf}}{\beta_{hnf}}\mathrm{Pr}\,Ra\theta,\end{aligned} \tag{9}$$

Energy:

$$U\frac{\partial\theta}{\partial X}+V\frac{\partial\theta}{\partial Y}+W\frac{\partial\theta}{\partial Z}=\frac{\alpha_{hnf}}{\alpha_{fluid}}\left(\frac{\partial^2\theta}{\partial X^2}+\frac{\partial^2\theta}{\partial Y^2}+\frac{\partial^2\theta}{\partial Z^2}\right), \tag{10}$$

Based on the above governing Eqns. (6)-(10), setting $\varepsilon=1, Da\to\infty$ i.e. unity porosity and infinite permeability one retrieves the case of flow in the hybrid nanofluid layer while values of ε less than unity and finite Da represent the flow in the porous layer. The previous system is solved subjected to the following boundary conditions:

$$\begin{aligned}&\text{on the side planes}: U=V=W=0, \quad \theta=0,\\ &\text{on the upper planes}: U=V=W=0, \quad \frac{\partial\theta}{\partial n}=0,\\ &\text{on the fin}: U=V=W=0, \quad \theta=1\end{aligned} \tag{11}$$

The correlations used to evaluate the thermophysical properties of the hybrid nanofluid are documented in **Table 1**. Based on these the appropriate values for the hybrid magnetic nanofluid considered in the simulations are given in **Table 2**.

Table 1. Thermo-physical relations for computing properties of the nanoparticles and base fluid.

Properties	**Hybrid nanofluid**	**Classical nanofluid**
Density	$\rho_{hnf}=(1-\varphi)\rho_{fluid}+\varphi\rho_{np}$	$\rho_{np}=\frac{\varphi_{Fe_3O_4}\rho_{Fe_3O_4}+\varphi_{MWCNT}\rho_{MWCNT}}{\varphi}$
Heat capacity	$(\rho c_p)_{hnf}=(1-\varphi)(\rho c_p)_{fluid}+\varphi(\rho c_p)_{np}$	$(c_p)_{np}=\frac{\varphi_{Fe_3O_4}(c_p)_{Fe_3O_4}+\varphi_{MWCNT}(c_p)_{MWCNT}}{\varphi}$
Coefficient of thermal expansion	$(\rho\beta)_{hnf}=(1-\varphi)(\rho\beta)_{fluid}+\varphi(\rho\beta)_{np}$	$\beta_{np}=\frac{\varphi_{Fe_3O_4}\beta_{Fe_3O_4}+\varphi_{MWCNT}\beta_{MWCNT}}{\varphi}$
Electrical conductivity	$\sigma_{hnf}=(1-\varphi)\sigma_{fluid}+\varphi\sigma_{np}$	$\sigma_{np}=\frac{\varphi_{Fe_3O_4}\sigma_{Fe_3O_4}+\varphi_{MWCNT}\sigma_{MWCNT}}{\varphi}$
Thermal conductivity	$k_{hnf}=\frac{k_{np}+(n-1)k_f-(n-1)(k_f-k_{np})\varphi}{k_{np}+(n-1)k_f+(k_f-k_{np})\varphi}k_f$	$k_{np}=\frac{\varphi_{Fe_3O_4}k_{Fe_3O_4}+\varphi_{MWCNT}k_{MWCNT}}{\varphi}$
viscosity	$\mu_{hnf}=\frac{\mu_f}{(1-\varphi)^{2.5}}$	$\varphi=\varphi_{MWCNT}+\varphi_{Fe_3O_4}$

Table 2. Thermo-physical properties of the nanoparticles and base fluid.

	Pure water	Fe_3O_4	*MWCNT*
$\rho\,(kg/m^3)$	997.1	5200	2100
$C_p(J/Kg\,K)$	4179	670	710
$k\,(W/mk)$	0.613	6	2000
$\beta\times10^{-5}\,(1/K)$	21	1.3	**?**
$\sigma\,(S/m)$	0.05	25000	**?**

A change in the amount of entropy in the flow of nanofluids is predicted. As there are also certain variations in thermal transport, it is possible to describe the *total entropy* [34-37] as follows:

$$S_{tot} = S_{ht} + S_{ff} + S_{mf} \tag{12}$$

$$S_{ht} = \frac{k_{hnf}}{T_0^2}\left[\left(\frac{\partial T}{\partial x}\right)^2 + \left(\frac{\partial T}{\partial y}\right)^2 + \left(\frac{\partial T}{\partial z}\right)^2\right] \tag{13}$$

$$S_{ff} = \frac{\mu_{hnf}}{T_0}\left[2\left(\left(\frac{\partial u}{\partial x}\right)^2 + \left(\frac{\partial v}{\partial Y}\right)^2 + \left(\frac{\partial w}{\partial z}\right)^2\right) + \left(\frac{\partial u}{\partial y} + \frac{\partial v}{\partial x}\right)^2 + \left(\frac{\partial w}{\partial y} + \frac{\partial v}{\partial z}\right)^2 + \left(\frac{\partial u}{\partial z} + \frac{\partial w}{\partial x}\right)^2\right] + \frac{\mu_{hnf}}{T_0 K}(u^2 + v^2 + w^2) \tag{14}$$

$$S_{mf} = \frac{\sigma_{hnf}}{T_0}\left(v \times \mathbf{B_0}\right)^2 \tag{15}$$

With $T_0 = \dfrac{T_C + T_h}{2}$, Entropy generation S_{tot} can be written in *dimensionless* form as follows

$$S_{TOT} = S_{HT} + S_{FF} + S_{MF} \tag{16}$$

$$S_{HT} = \frac{k_{hnf}}{k_{fluid}}\left[\left(\frac{\partial \theta}{\partial X}\right)^2 + \left(\frac{\partial \theta}{\partial Y}\right)^2 + \left(\frac{\partial \theta}{\partial Z}\right)^2\right] \tag{17}$$

$$S_{FF} = \frac{\mu_{hnf}}{\mu_{fluid}} N_\mu \left\{\begin{array}{l}\left[2\left(\frac{\partial U}{\partial X}\right)^2 + 2\left(\frac{\partial V}{\partial Y}\right)^2 + 2\left(\frac{\partial W}{\partial Z}\right)^2\right] \\ + \left(\frac{\partial^2 U}{\partial Y^2} + \frac{\partial^2 V}{\partial X^2}\right)^2 + \left(\frac{\partial^2 W}{\partial Y^2} + \frac{\partial^2 V}{\partial Z^2}\right)^2 + \left(\frac{\partial^2 U}{\partial Z^2} + \frac{\partial^2 W}{\partial X^2}\right)^2\end{array}\right\} + \frac{\mu_{hnf}}{\mu_{fluid}} N_\mu \left(\frac{U^2 + V^2 + W^2}{Da}\right) \tag{18}$$

$$S_{MF} = N_{\mu}\frac{\sigma_{hnf}}{\sigma_{fluid}}Ha^2\left(U^2+V^2\right) \tag{19}$$

Here, in the hybrid nanofluid layer, $Da \to \infty$. The local and average Nusselt numbers (dimensionless heat transfer rates adjacent to the rectangular hot obstacle), Nu_{loc} and Nu_{avg} are estimated as:

$$\begin{aligned} Nu_{loc} &= -\frac{k_{eff}}{k_{fl}}\left(\frac{\partial\theta_{po}}{\partial n}\right)_{wall}, \\ Nu_{avg} &= \frac{1}{S^2}\int_0^s\int_0^s Nu_{loc}\,dydz \end{aligned} \tag{20}$$

3. COMSOL Finite Element Solution Methodology

The dimensionless governing equations of Eqs. (6) – (10) regulated by the assumed boundary conditions are highly nonlinear and strongly coupled. COMSOL Multiphysics software platform [38, 39] is therefore adopted for a numerical solution. This deploys the Galerkin weighted and finite element resolution techniques. The adopted Galerkin weighted residual method very effectively accommodates the governing equations. These are formulated as integral mathematical equations. The first step is the *discretization process* of the computational domain into small triangular elements, as illustrated in Fig. 2 (b). Lagrangian triangular finite elements about multiple shapes are applied to different regions inside the computational region. The residuals for any conservation equation are reached by replacing the approximations of the dimensionless governing equations. To deal with the nonlinear expressions in the momentum equations (7-9), a Newton-Raphson iteration algorithm is employed. Convergence concerning the solution is only adequate if the following convergence criteria for the relative error of each variable is achieved:

$$\left|\frac{\Gamma^{i+1}-\Gamma^{i}}{\Gamma^{i+1}}\right| \le \eta \tag{21}$$

Here i indicate the iteration value and η represents the convergence criterion. In this numerical study, the convergence criterion is defined as $\eta = 10^{-6}$. COMSOL platform features porous media, heat transfer and also magnetohydrodynamics options and is very adaptive and user-friendly [40].

4.Validation of COMSOL finite element solutions

To verify the accuracy of the COMSOL computations, benchmarking against the experimental study of Krane and Jesee [40] for the special case of *non-magnetic viscous Newtonian natural convection in a vertical square enclosure containing water* (*Pr* = 7.0, infinite permeability and vanishing magnetic field and absence of nanoparticles). The comparison for temperature at the left hot wall is given in **Figure 2** below and excellent agreement is obtained confirming the accuracy of the COMSOL finite element code deployed.

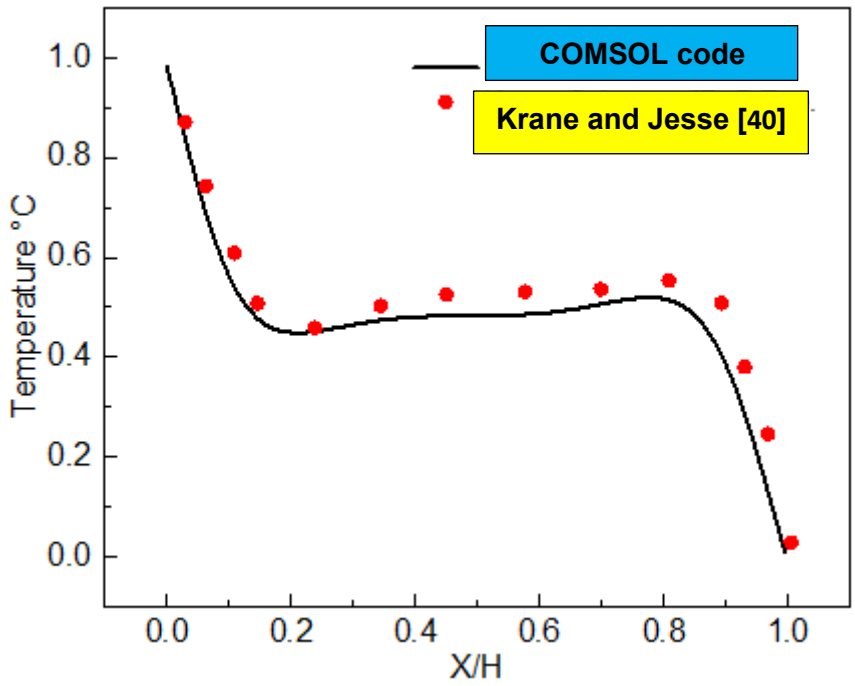

Fig.2 Comparison of the current COMSOL solutions with Krane & Jesse [40]

5.Graphical Results and Discussion

Extensive visualization of COMSOL finite element solutions is given in **Figures 3 - 15**.

Fig. 3 shows the 3-D contour plots for streamlines (isovels), isotherms and Bejan (entropy) number with the influence of *Darcy number* and all other parameters fixed. The Darcy number features in the dimensionless momentum equations as a reciprocal in both the Darcian linear impedance term and the quadratic Forchheimer (inertial drag) term. Each momentum equation contains the appropriate version of these terms in the respective velocity component i. e. *U, V, W*. Evidently at low *Da* values ($Da = 10^{-5}$, $Da = 10^{-4}$) there is a significant contribution from both the Darcy impedance and the Forchheimer resistance. This corresponds to very low permeabilities of the porous layer in the trapezoidal configuration. With greater Darcy number,

both linear and quadratic drag forces are reduced and this induces significant acceleration in the enclosure, as evident in the intensification in streamlines at $Da = 10^{-2}$ and the emergence of red higher velocity zones both adjacent to the fin and at the sloping walls. A dual vortex cell structure is also computed for all cases on either side of the fin, although it is most prominent at maximum Darcy number. Isotherms are also strongly influenced by increment in Darcy number. The cooler blue zones immediately above the central cylindrical fin are replaced with warmer green zones. There is also a stronger presence of red hotter zones in the magnetic nanofluid at the periphery of the fin and these grow laterally to encompass the wavy wall zone at the base of the enclosure with greater Darcy number.

	streamlines	**isotherm**	**Bejan number**
Da= 10^{-5}	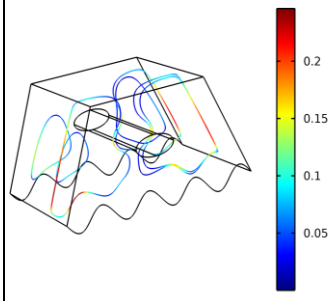	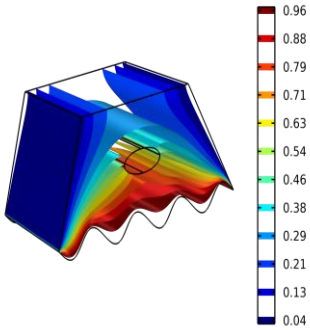	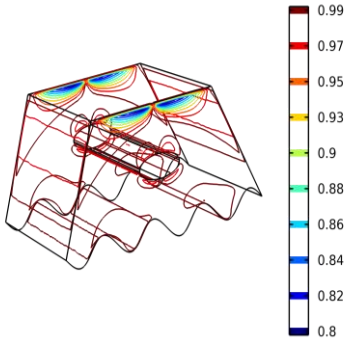
Da= 10^{-4}	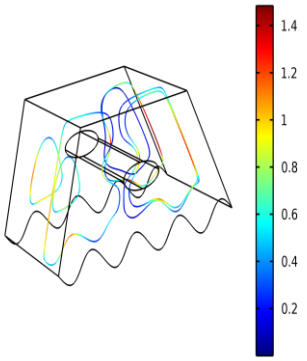	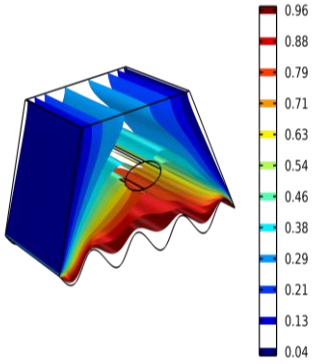	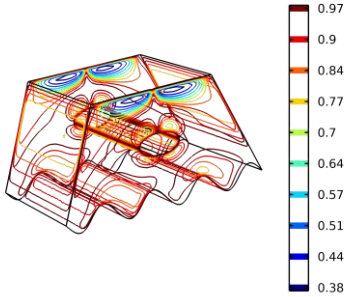
Da= 10^{-3}	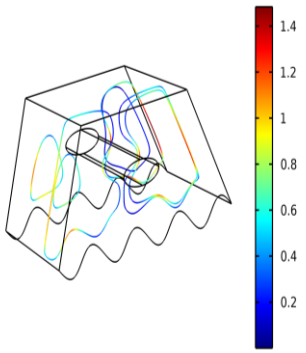	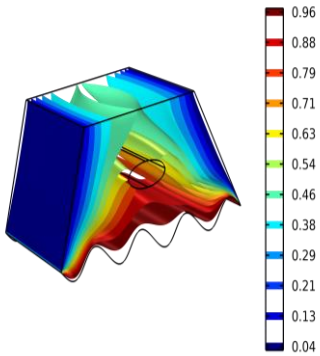	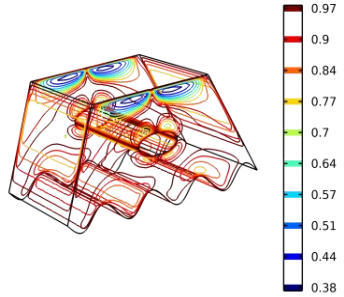

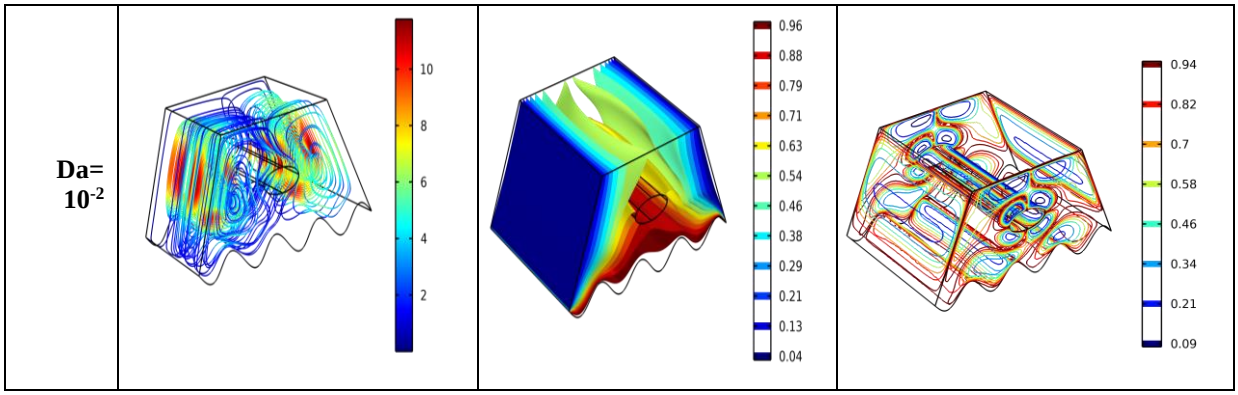

Fig. 3. Distribution of the velocity, temperature and Bejan number for Da in different scenarios

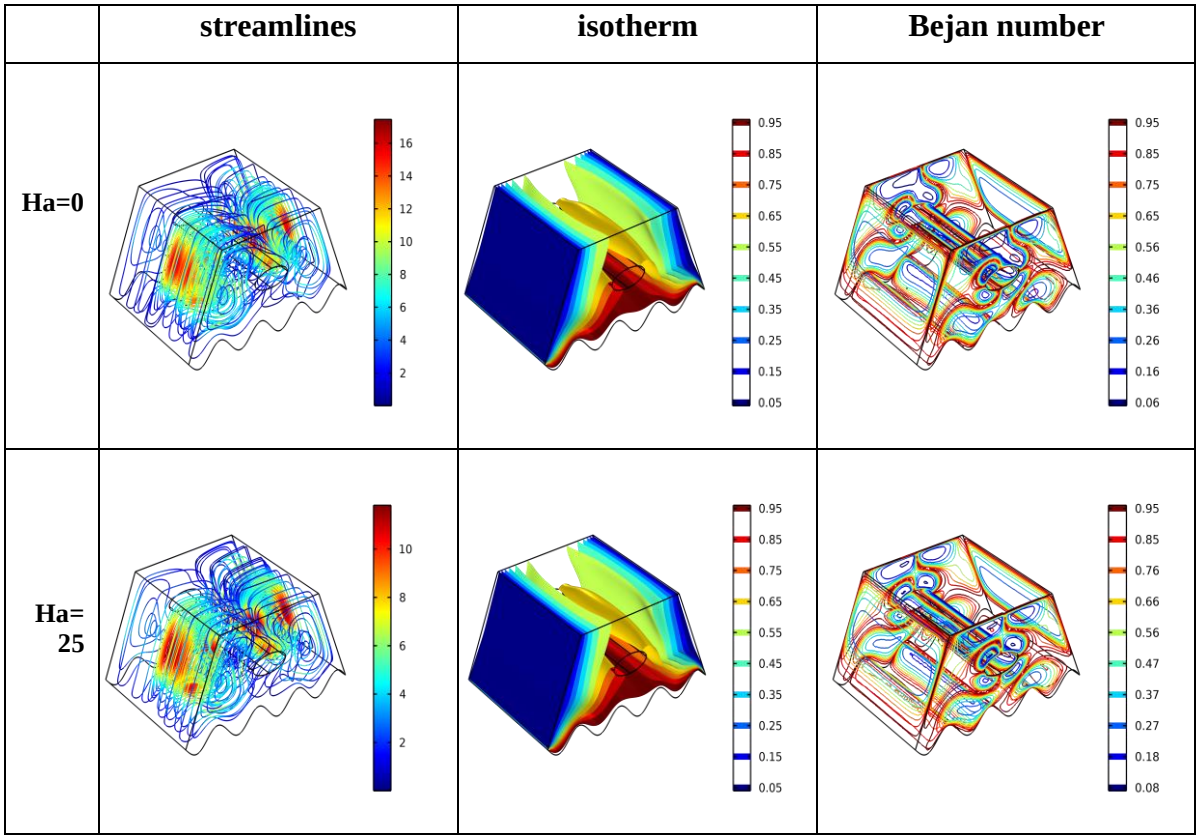

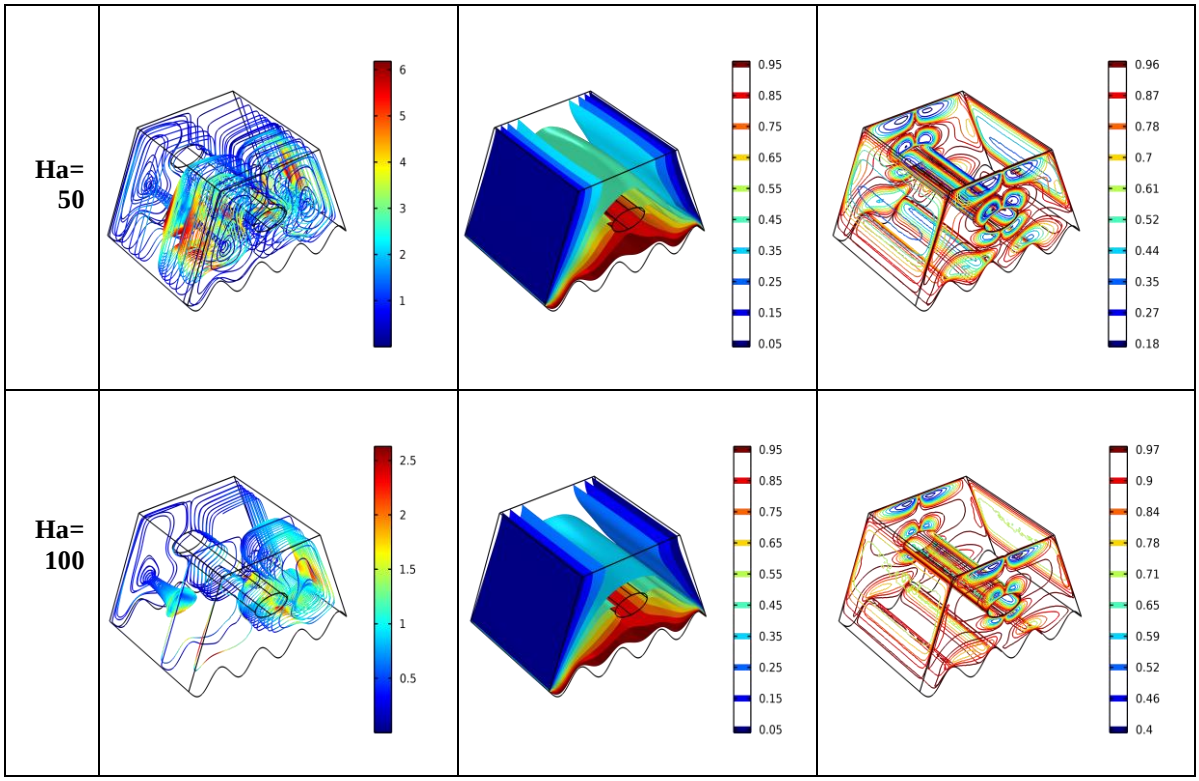

Fig. 4. Distribution of the velocity, temperature and Bejan number for Ha in different scenarios

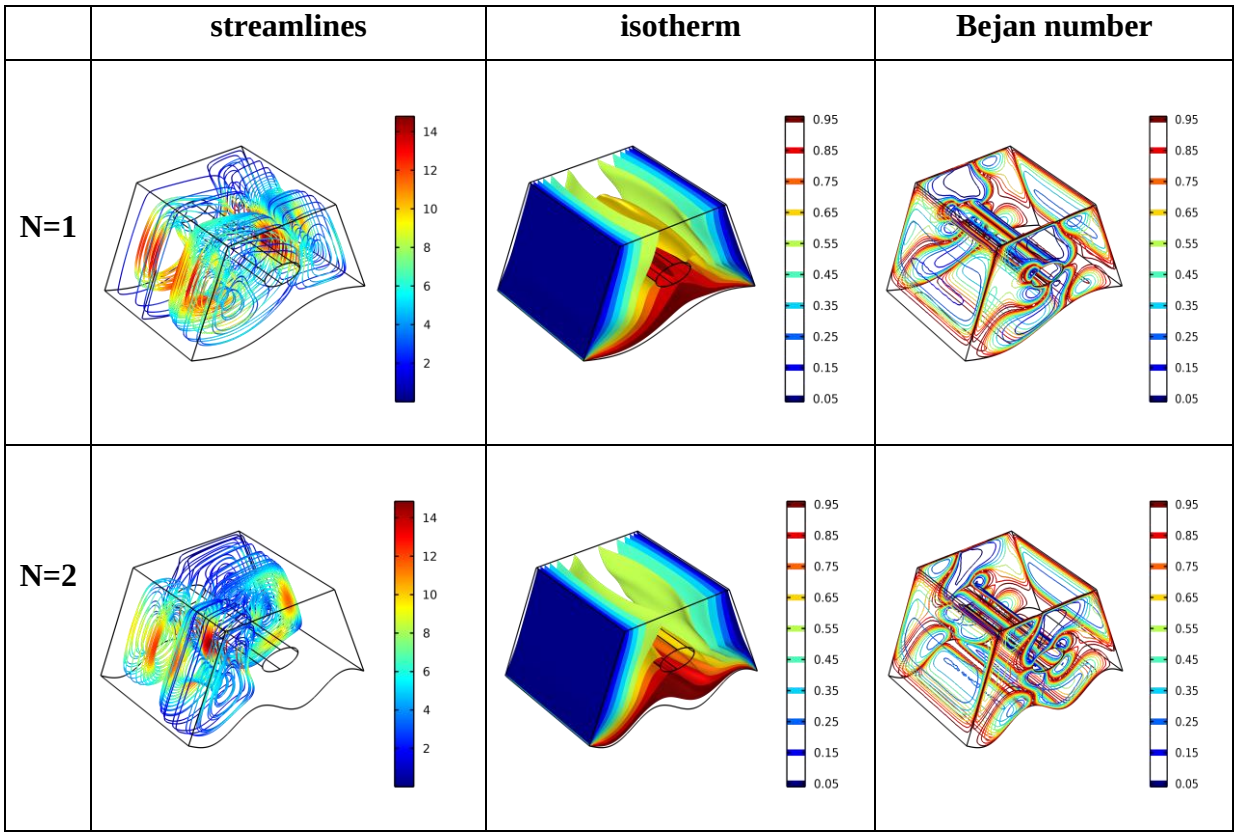

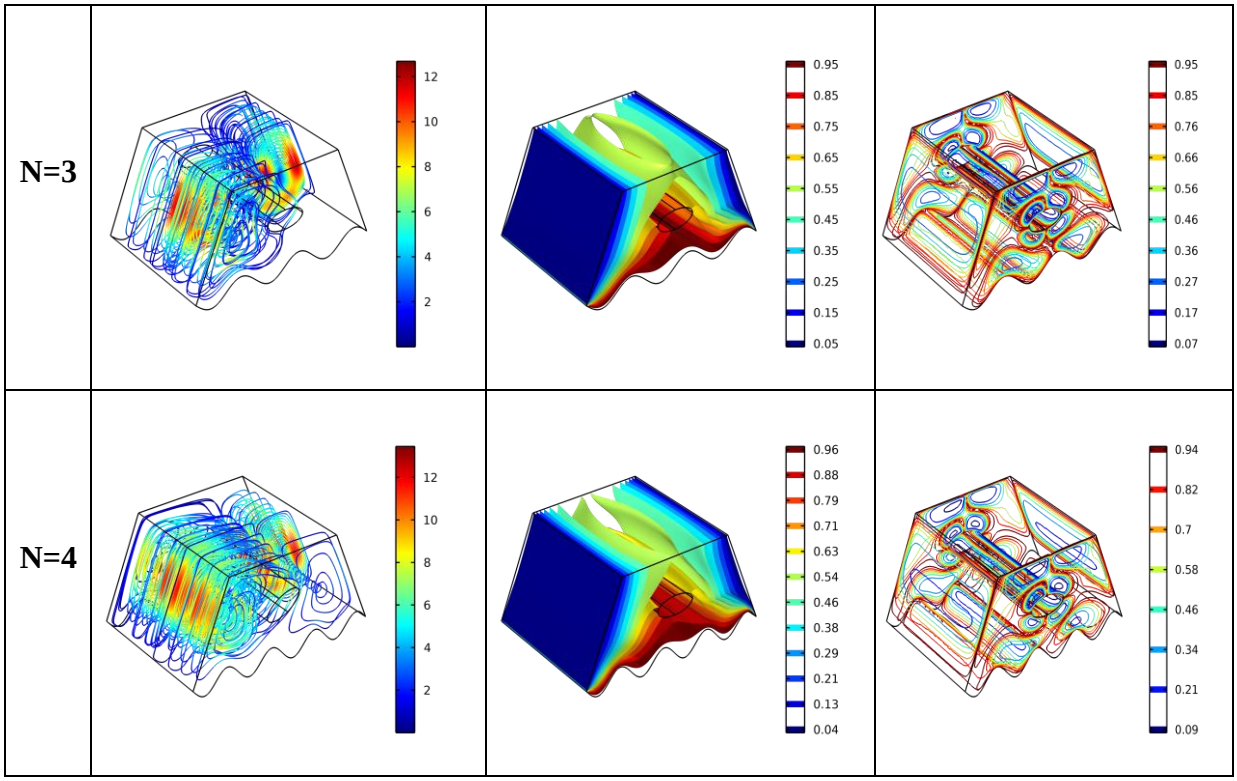

Fig. 5. Distribution of the velocity, temperature and Bejan number for N in different scenarios

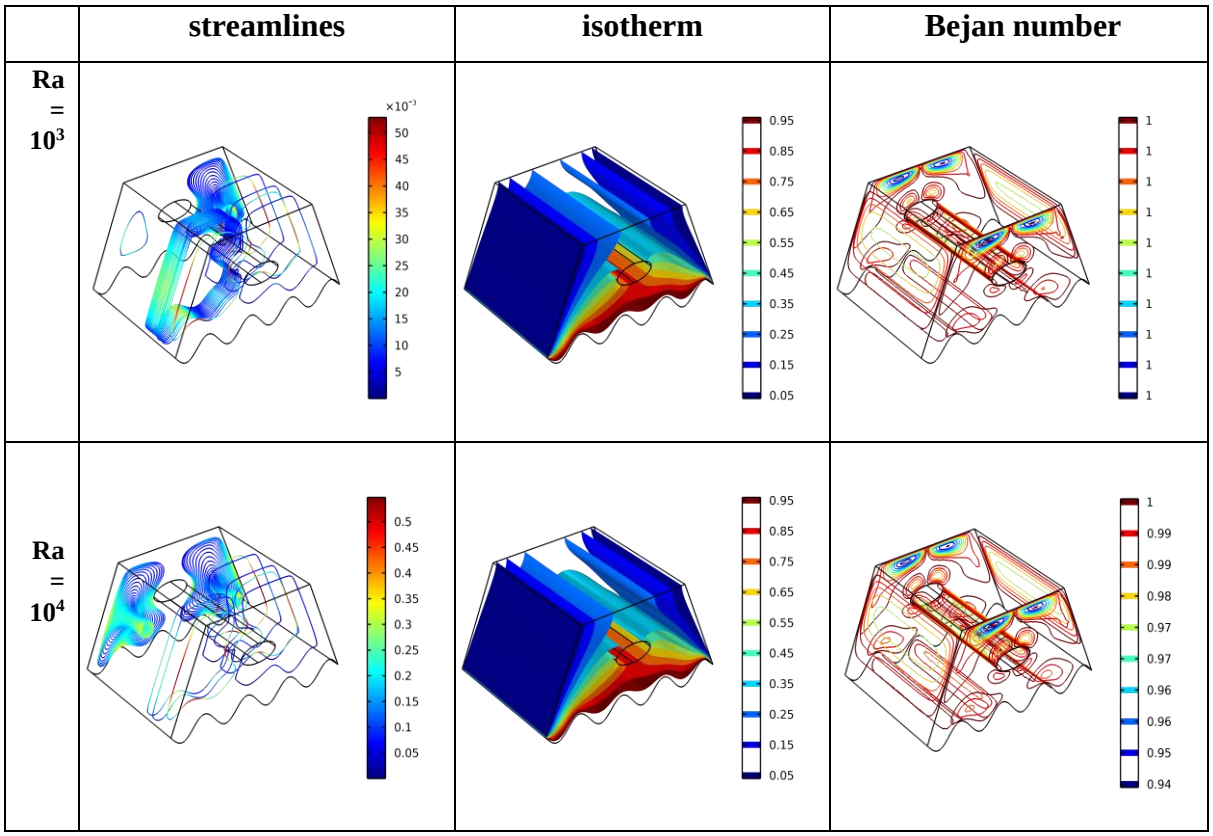

Ra = 10^5	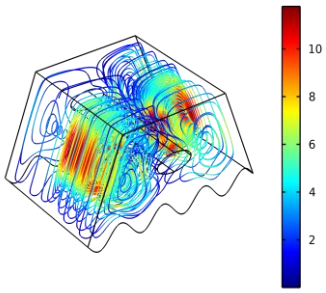	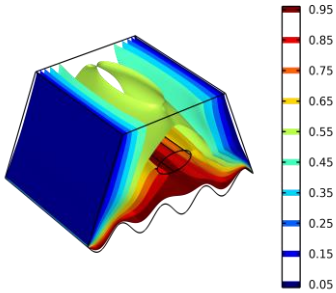	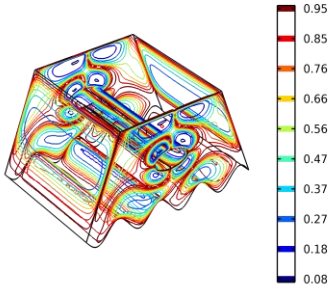
Ra = 10^6	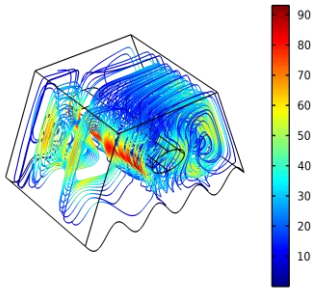	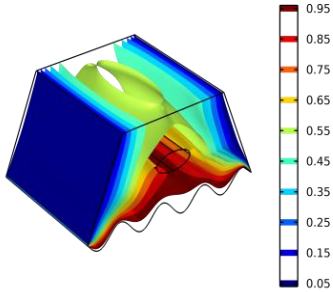	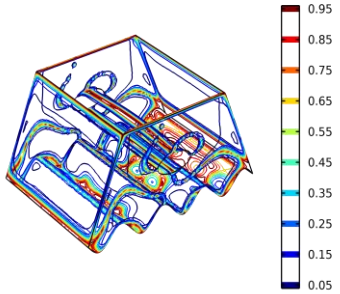

Fig. 6. Distribution of the velocity, temperature and Bejan number for Ra in different scenarios

	streamlines	**isotherm**	**Bejan number**
$\gamma = 0$	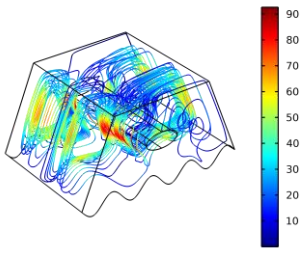	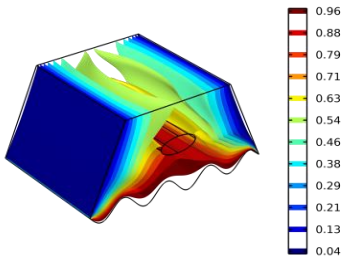	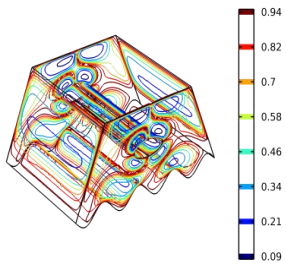
$\gamma = 30$	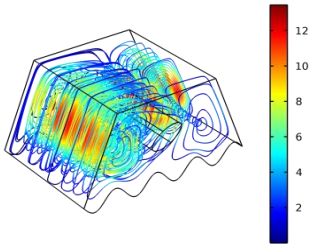	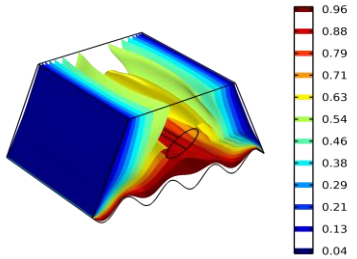	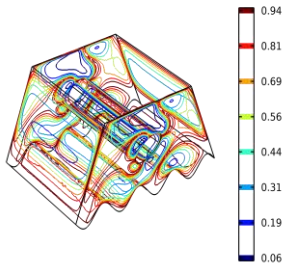

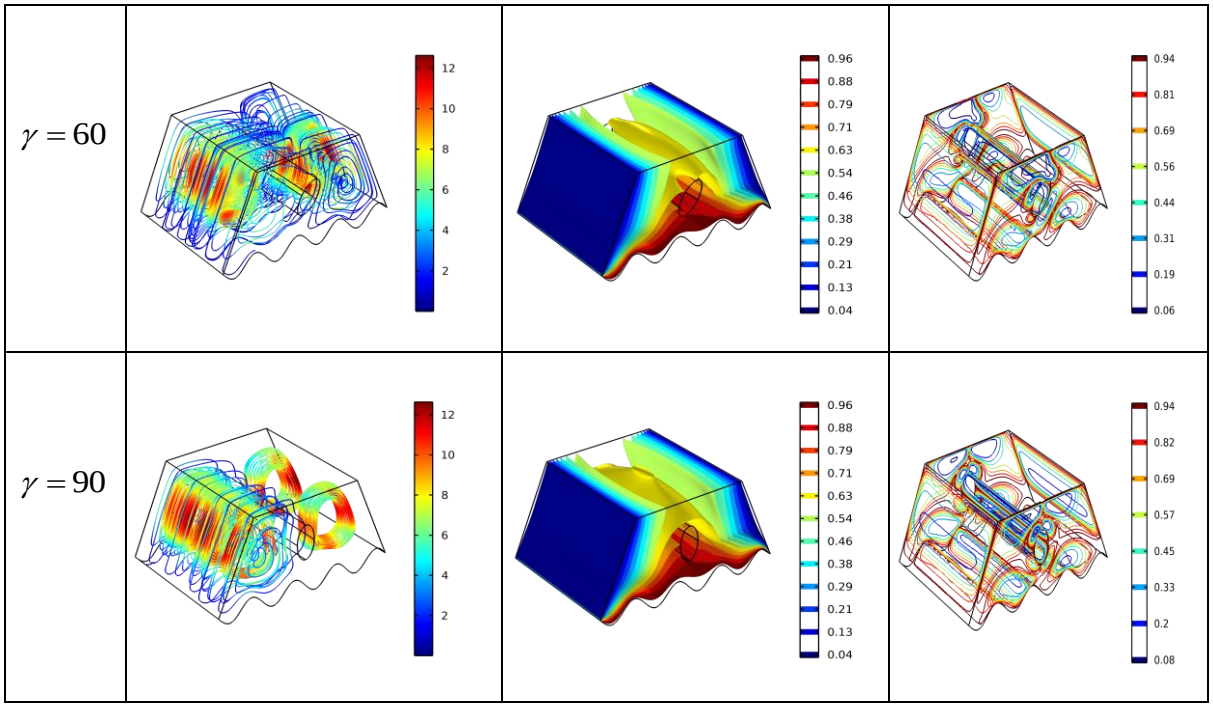

Fig. 7. Distribution of the velocity, temperature and Bejan number for γ in different scenarios

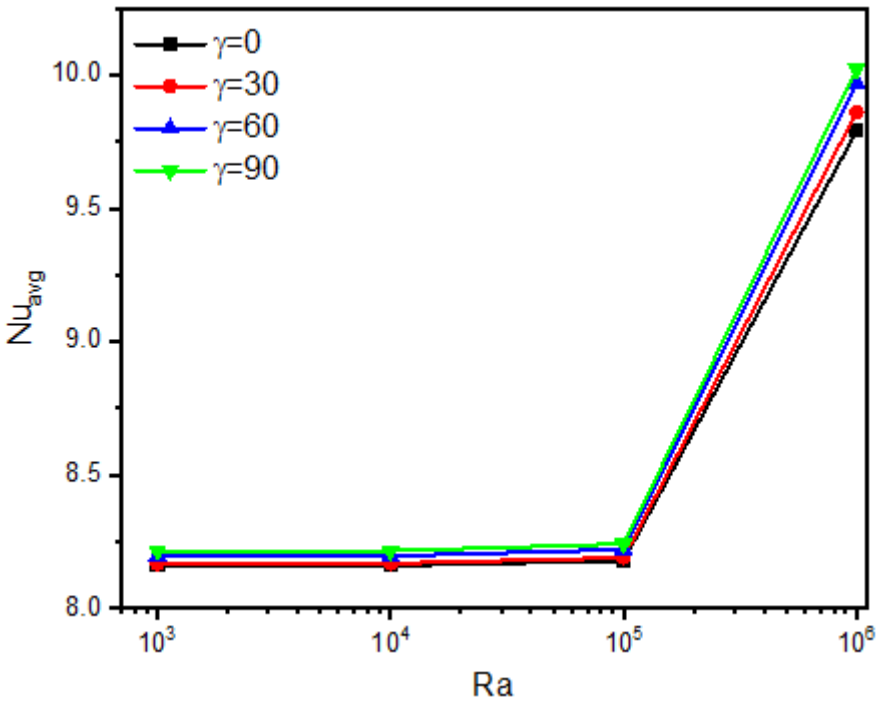

Fig. 8. Average Nusselt number versus Rayleigh number adjacent to obstacle for different volume fractions

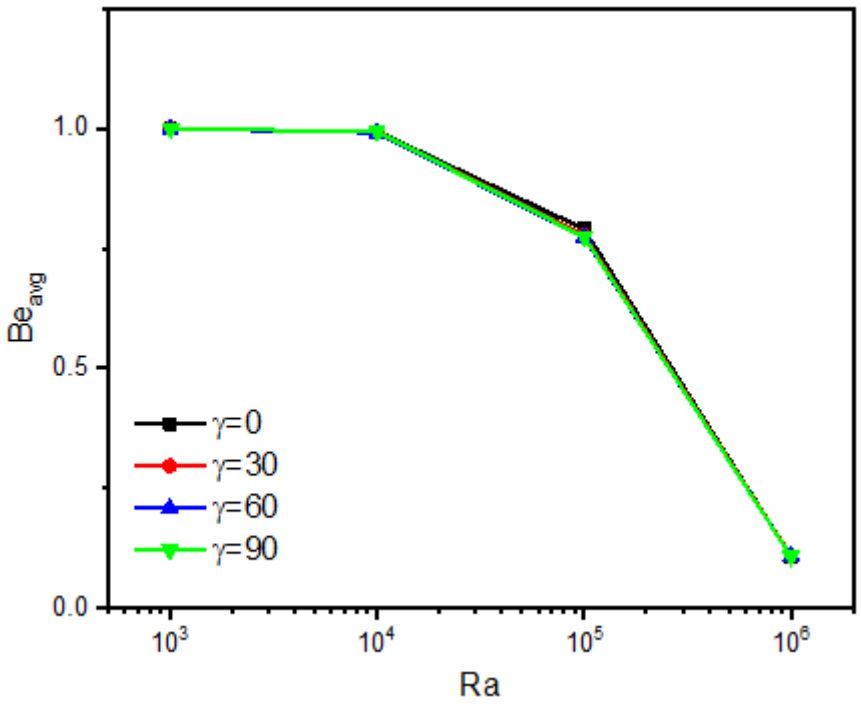

Fig. 9. Average Bejan number versus Rayleigh number adjacent to obstacle for different volume fractions

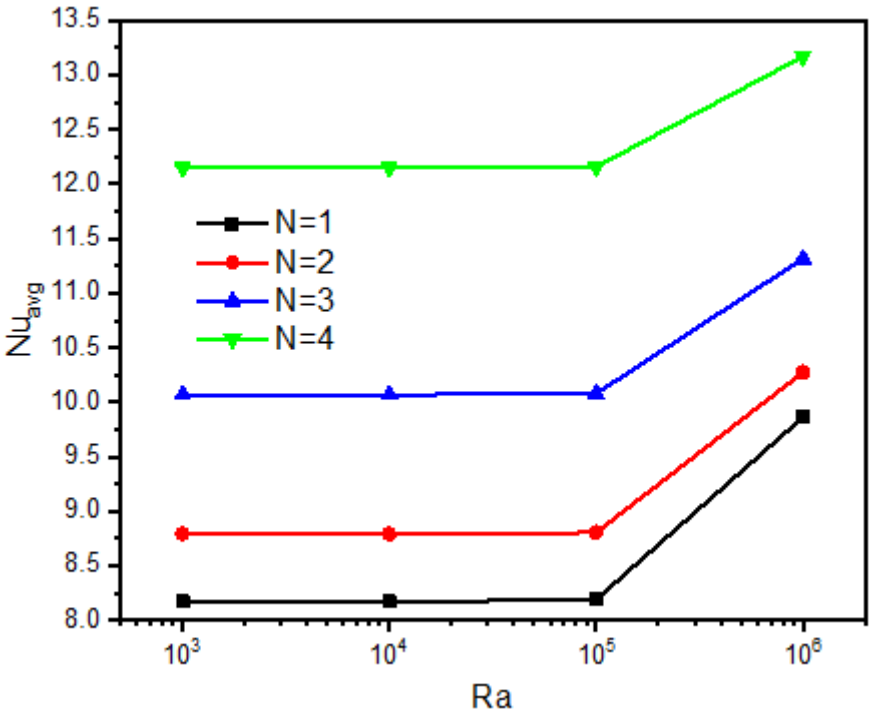

Fig. 10. Average Nusselt number versus Rayleigh number for different undulation numbers of wavy wall

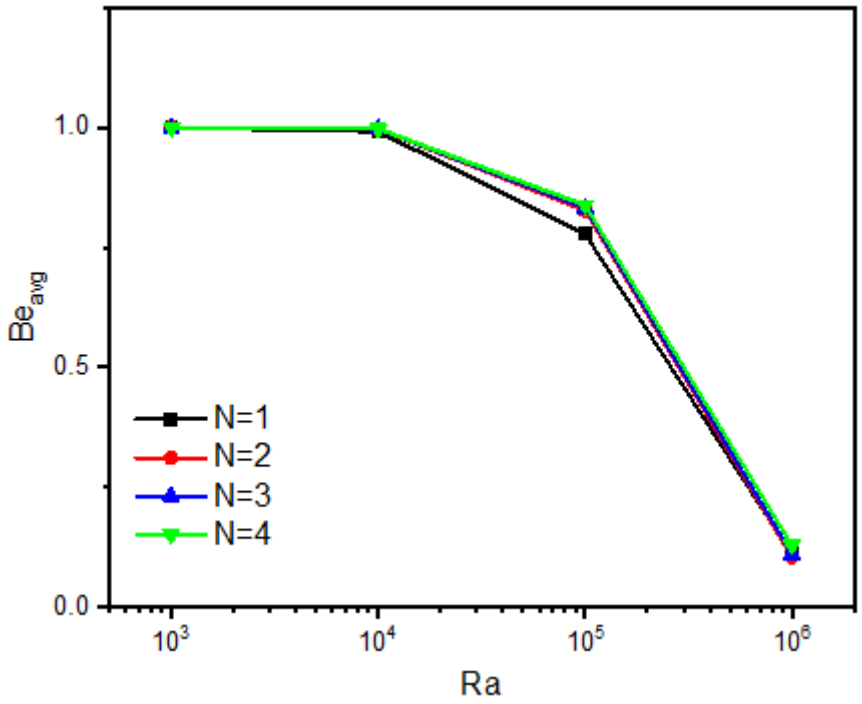

Fig 11. Average Bejan number versus Rayleigh number for different undulation numbers of wavy wall

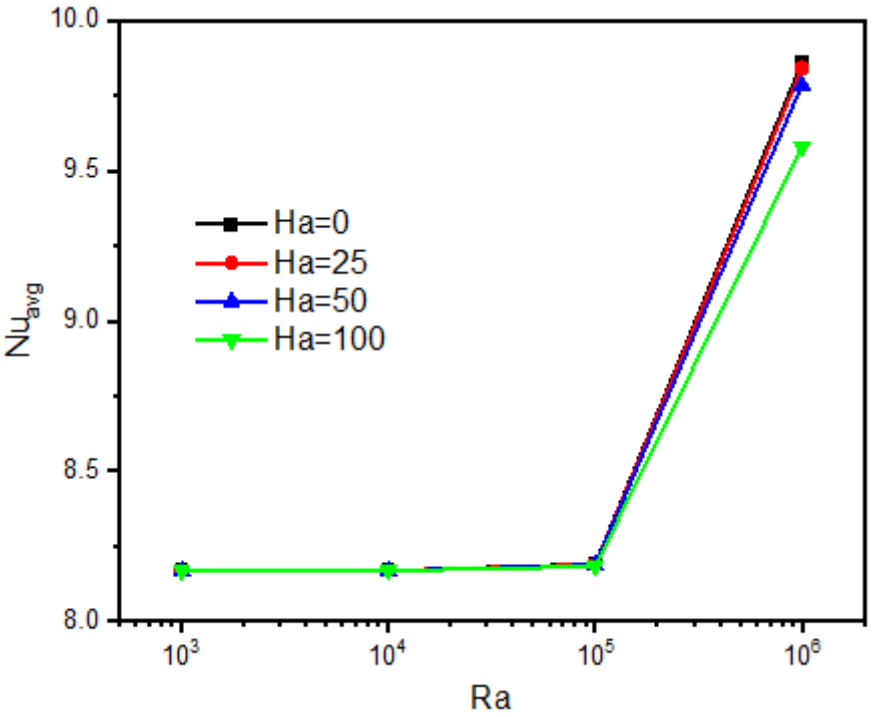

Fig 12. Average Nusselt number versus Rayleigh number for different Hartmann magnetic numbers

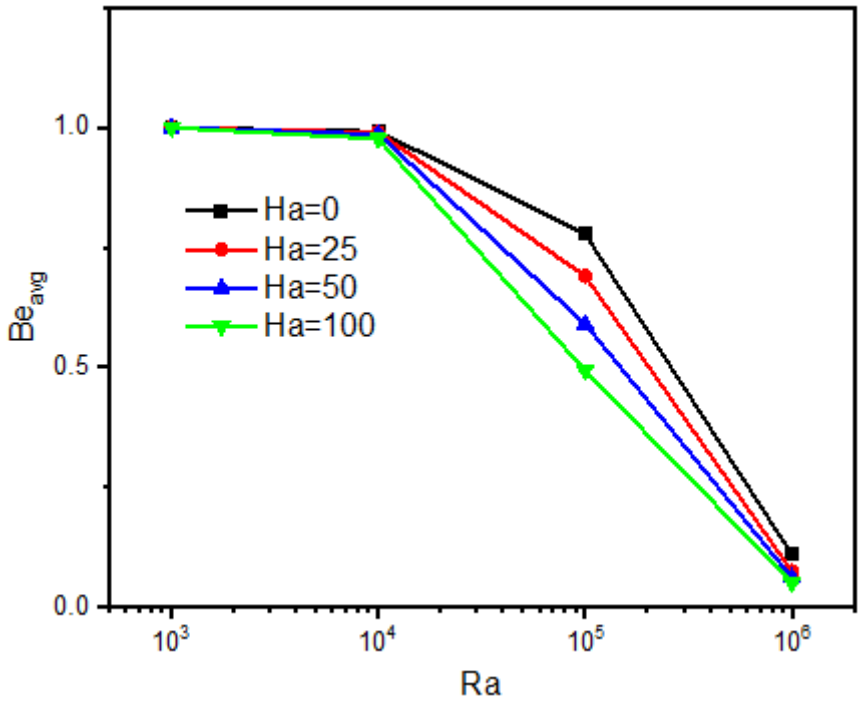

Fig 13. Average Bejan number versus Rayleigh number for different Hartmann magnetic numbers

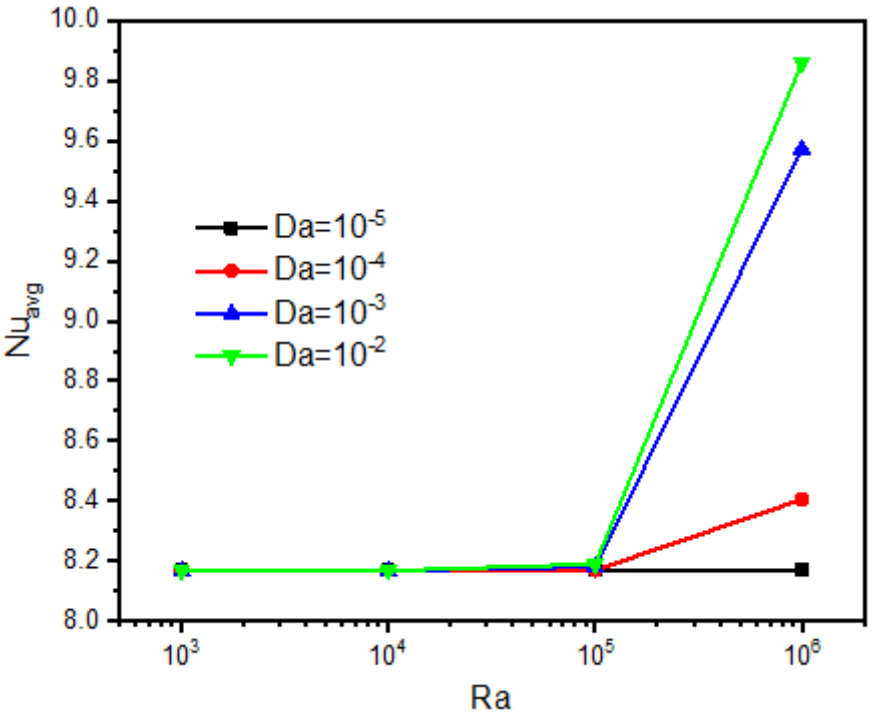

Fig 14. Average Nusselt number versus Rayleigh number for different Darcy numbers

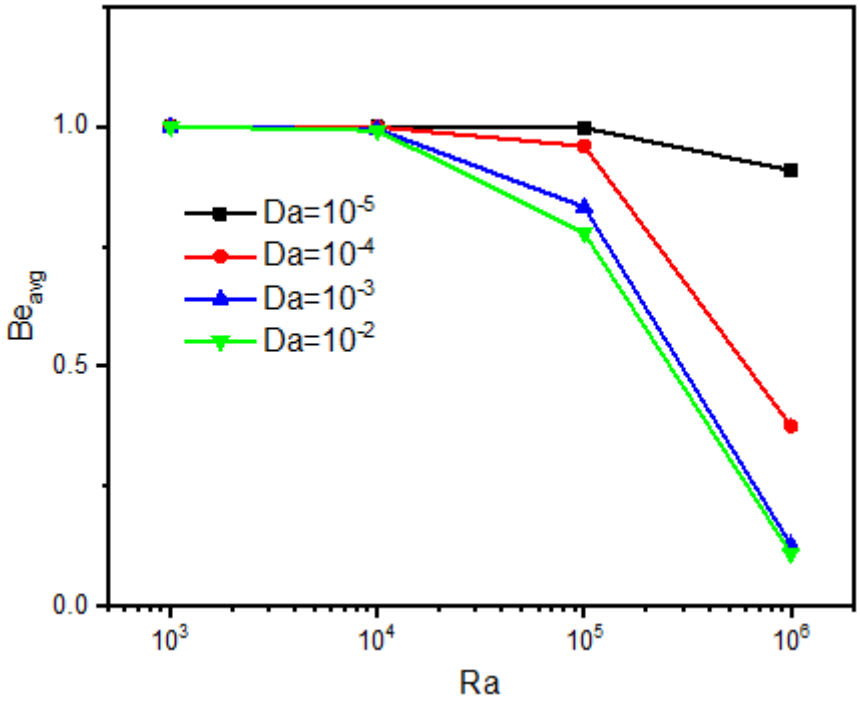

Fig 15. Average Bejan number versus Rayleigh number for different Darcy numbers

The reduction in permeability of the porous medium therefore serves as an excellent mechanism for exacerbating convective heat transfer in the enclosure. Bejan number contours are also markedly influenced with increment in Darcy number. Bejan number is a very useful dimensionless number in second law thermodynamic analysis and optimization of thermal systems. It quantifies the ratio of *thermal entropy generation* to the *total entropy generation (thermal and frictional)*. Therefore, the Bejan number has no effect on heat transfer but rather is a description of the entropy generated by heat transfer *and* fluid friction. For any thermal system, when Bejan values are close to one, this indicates that thermal entropy generation is predominant on the total entropy generation compared with frictional entropy generation. When heat transfer is intensified (as observed in the isotherms), Nusselt numbers will be elevated. This will imply a reduction in entropy generation and a decrease in Bejan number. Nusselt number quantifies the heat transfer rate whereas Bejan number shows the irreversibilty due to heat transfer. Clearly the irreversibilty in the trapezoidal enclosure decreases as the heat transfer rate (and isotherm magnitudes) increase. The predominantly red contours for Bejan number at lower Darcy numbers are replaced with a significantly greater presence of blue and green (lower magnitudes) at highest Darcy number. This indicates that lower permeability

(high Darcy number) suppresses the entropy generation in the system which is much larger for higher permeability (low Darcy number).

Fig. 4 shows the 3-D contour plots for streamlines (isovels), isotherms and Bejan (entropy) number with the influence of *Hartmann magnetic number* and all other parameters fixed. The Hartmann number features in the dimensionless momentum equations in the linear Lorentzian magnetic body force term. For example, in the *X*-direction momentum equation (7), this term appears as $-\frac{\sigma_{hnf}}{\sigma_{fluid}}\frac{Pr\,Ha^2}{\varepsilon}\boldsymbol{U}$. $Ha = LB\sqrt{\frac{\sigma_{nf}}{\mu_{nf}}}$ and embodies the relative influence of the hydromagnetic body force (Lorentz force) to the viscous resistance in the magnetic nanofluid. When $Ha \rightarrow 0$, magnetic field effects are negated and the *electrically non-conducting viscous nanofluid case* is retrieved. For *Ha = 1* both magnetic and viscous forces contribute equally. For *Ha* >>1 i. e. *Ha* = 25, 50 and 100, the magnetic body force is dominant and exerts a significant damping effect on the internal flow. This explains the progressive elimination in yellow and red higher velocity zones in the trapezoidal enclosure observed at *Ha* = 0 which are systematically diminished and almost completely vanish for *Ha* = 100. Blue low velocity contours proliferate at higher *Ha* values and this verifies the exceptional damping (flow control) achieved in internal circulation dynamics of enclosures with stronger transverse magnetic field. The dual vortex structure is sustained for *Ha* = 0, 25, 50; however, at *Ha* = 100 it is clearly disrupted and essentially reduced in size being localized to the back left corner and forward right corner. Vorticity is therefore very strongly suppressed with intense magnetic field. Isotherms are observed to be depleted in magnitude however with increasing magnetic field effect i.e. greater Hartmann number. At *Ha* = 0 there are significant yellow and green zones featured in the zone above the fin and these penetrate and develop into hotter red zones between the fin and the wavy base wall. As *Ha* is increased however the yellow warmer zones are replaced with cooler green and blue (*Ha* = 50) and eventually completely blue cold zones (*Ha* =100). However, there is intensification beneath the fin and isotherms have higher magnitudes in the lower hotter zones compared to the cases with lower Hartmann number. Convective heat transfer is therefore intensified in the lower section of the enclosure and this is attributable to the dissipation of supplementary work expended in dragging the magnetic fluid against the action of the transverse magnetic field which is dissipated as heat. This kinetic energy dissipation produces temperature enhancement which is a characteristic of magneto-convective flows, as noted by Cramer and Pai [41], among others. There is a marginal reduction in Bejan number contour intensity with greater magnetic field at lower *Ha* values; however the

emergence of stronger red zones at higher Ha values indicates that Bejan entropy number is elevated with magnetic field intensity since frictional effects due to the magnetic body force impedance are much greater.

Fig. 5 visualizes the 3-D contour plots for streamlines (isovels), isotherms and Bejan (entropy) number with the influence of *wavy surface undulation number (N)* and all other parameters fixed. This parameter arises in the eqn. (1), $x = -A\sin\left(\frac{N\pi x}{H}\right)$ and is the principal mechanism quantifying the effect of the waviness of the base wall on the internal convection regime. With increasing *N*, streamlines are considerably influenced. The left vortex cell is intensified whereas the right vortex cell is constrained and forced increasingly towards the back wall of the trapezoidal enclosure. There is a dramatic emergence of red higher velocity zones at the left sloping wall which is maximized at *N* = 4. Strong intensification in the right-side vortex is also sobered and this cell in fact splits into two discrete sub-vortex structures at *N* = 3. Clearly, the number of undulations on the base wall therefore imparts a significant modification in the internal flow structure. Isotherms are also modified with increasing *N*. The dominant warmer yellow/orange zones above the fin at low *N* values are replaced progressively with cooler green zones and the hotter base zone above the wavy wall is also slightly cooled. Bejan number contours are also modified (relaxed) at the back wall of the trapezoidal enclosure with increasing *N* values and there is a marginal intensification near the front wall and in the vicinity of the fin.

Fig. 6 displays the 3-D contour plots in the trapezoidal enclosure for streamlines (isovels), isotherms and Bejan (entropy) number, respectively with the influence of *Rayleigh number (Ra)* and all other parameters fixed. This parameter arises solely in the Z-direction momentum eqn. (9), in the term, $+\frac{\beta_{hnf}}{\beta_{hnf}} Pr\, R\, a\theta$. It effectively couples the momentum field with the energy equation (10). $Ra = \frac{g\beta_{fluid}(T_h - T_c)L^3}{\alpha_{fluid}\nu_{fluid}}$ and embodies the relative contribution of the thermal buoyancy force to the viscous hydrodynamic force. When *Ra* = 0 the case of forced convection is retrieved i.e. thermal buoyancy vanishes. When *Ra* = 1 both forces contribute equally. For strong natural convection, values have been prescribed from *Ra* = 10^3 and upwards. With increasing Ra values, the dual vortex structure in the enclosure is synthesized progressively and high velocity (red) zones appear on either side of the fin. At maximum Ra (=106), at which point turbulence effects can be invoked, there is a strong distortion and acceleration (red zones near the fin periphery) in the left vortex cell and relaxation (and deceleration) in the right vortex

cell (blue zones dominate). Generally thermal buoyancy has a major influence on the circulation phenomena within the enclosure. Isotherms are also affected considerably with greater Rayleigh number. Strong temperature enhancement is produced at the upper zone of the enclosure above the fin (green contours replace blue ones) and there is a strong heating effect also near the fin edge and in the zone immediately above the wavy wall. Thermal buoyancy therefore encourages convective heat transfer in the regime. Significant modifications in Bejan entropy contours are also observed with increment in Rayleigh number. The blue lower value Bejan number contours at the upper back wall morph into red contours. However, in the vicinity of the fin, higher Bejan values are replaced with lower ones with higher Rayleigh number. Entropy production is therefore suppressed near the fin and in particular between the fin and the wavy base wall with greater thermal buoyancy effects.

Fig. 7 displays the 3-D contour plots in the trapezoidal enclosure for streamlines (isovels), isotherms and Bejan (entropy) number, respectively with the influence of volume fraction *(ϕ)* and all other parameters fixed. This parameter enables the doping of the nanoparticles to be simulated in the circulating magnetic fluid in the enclosure. With increasing volume fraction, the vortex structures (streamlines) are intensified in particular on the left-hand side of the cavity. Stronger red high velocity zones are computed near the left sloping wall. Higher red and yellow velocity zones also appear at the periphery of the fin. The right-hand side vortex is however decelerated owing to momentum conservation and finally splits into two distinct vortex ring structures at very high values of volume fraction. Increasing volume fraction also induces significant heating in the enclosure with the cooler green upper zones systematically evolving into orange and yellow zones above the fin. Red high temperature zones are also observed increasingly around the fin and in the space above the wavy wall, confirming that increasing nanoparticle presence in the hybrid nanofluid achieves the desired thermal enhancement. Bejan number contour magnitudes are gradually depleted especially near the fin upper surface and sloping walls i.e. they morph from red and yellow contours to blue ones with increasing volume fraction.

Figs. 8-15 illustrate the variation in average Nusselt number (Nu_{avg}) and average Bejan number (Be_{avg}) with Rayleigh number and other selected parameters. These plots correspond to the fin outer wall i.e. the obstacle. **Fig. 8** shows that initially there is a weak elevation in average Nusselt number with increment in nanoparticle volume fraction. However, at Ra = 10^5, the plots dramatically increase in gradient and the effect of increasing volume fraction ins more significant. **Fig. 9** shows that the opposite behaviour is induced in the average Bejan number

i.e. it is reduced with greater nanoparticle volume fraction and also reduced consistently with greater Rayleigh number. Greater doping of the magnetic nanofluid and stronger thermal buoyancy effect therefore both deplete the entropy generation i.e. Be_{avg} in the trapezoidal enclosure. Clearly the generally inverse relationship between convective heat transfer and entropy generation is confirmed. Clearly **Fig. 10** displays that with increasing wavy base wall undulation number, there is a very significant increase in average Nusselt number, and this is sustained at all Rayleigh numbers, although a much steeper ascent in Nu_{avg} is observed after $Ra = 10^5$ (very strong thermal buoyancy). **Fig. 11** illustrates that there is a very weak increase in average Bejan number with increment in wavy base wall undulation number, up to Rayleigh number of $Ra = 10^4$; thereafter a more substantial increase is observed with greater N values, although the deviation is again suppressed as Ra approaches the maximum value of 10^6. **Figs. 12-13** present the evolution in average Nusselt number and average Bejan number with different Hartmann number (*Ha*) and Rayleigh number (*Ra*). With increase in *Ha i.e. stronger transverse magnetic field*, up to $Ra = 10^5$, there is no tangible alteration in average Nusselt number (Fig. 12). However, for $Ra > 10^5$, there graphs ascend very sharply and there is a plummet in average Nusselt number. The heating induced in the enclosure with greater magnetic field, as explained earlier, implies greater transfer of heat from the obstacle (fin) to the engulfing magnetic nanofluid. This indicates a reduction in heat transfer from the magnetic nanofluid to the wall (obstacle surface) which manifests in a depletion in average Nusselt number. Similarly, there is a depletion in entropy generation observed in Fig. 13 i.e. decrease in average Bejan number with increasing Hartmann number. However this behaviour is only computed for $Ra > 10^4$; for lower values of Rayleigh number the reduction in average Bejan number with stronger magnetic field intensity (i.e. higher *Ha*) values is trivial. Effectively stronger magnetic field is found to reduce average Nusselt number and also average Bejan number, but only beyond a critical Rayleigh number value which is different for each (it is lower for the average Bejan number plots and higher for the average Nusselt number plots). Both average Nusselt number and average Bejan number are maximum for the electrically non-conducting case i. e. $Ha = 0$.

Finally, **Figs. 14-15** depict the impact of Darcy number and Rayleigh number on the average Nusselt number and average Bejan number. With increase in *Da i. e. greater permeability of the porous medium and therefore lower Darcy and Forchheimer drag effects,* up to $Ra = 10^5$, there is no significant change in average Nusselt number (Fig. 14). However, for $Ra > 10^5$, a very sharp ascent is computed in profiles and substantial elevation in average Nusselt number with greater Darcy number is observed. Since temperatures are reduced with increasing Darcy

number owing to the progressive decrease in thermal conduction with the presence of less solid fibers in the porous medium (with higher permeability solid fibers in the porous medium matrix are decreased), this will correspond to a cooling of the regime. Therefore, *greater heat transfer away from the magnetic nanofluid saturated porous medium to the boundary* will be produced i. e. *average Nusselt number will be enhanced* as confirmed in Fig. 14. The opposite trends are witnessed for the average Bejan number (Fig. 15) where a strong suppression in average Bejan number accompanies an increase in Darcy number. However, this again is only achieved beyond a critical Rayleigh number i.e. $Ra > 10^4$, prior to which there is no modification in average Bejan number.

6.Conclusions

A theoretical and numerical analysis of the performance of electrically conducting water-Fe_3O_4/CNT hybrid nanofluid materials in three-dimensional natural convective heat transfer and entropy generation under transverse magnetic field within a wavy-walled trapezoidal enclosure has been conducted. The enclosure has two layers - a hybrid nanofluid layer and a porous medium layer. Newtonian flow is considered and the modified Navier-Stokes equations are employed with Lorentz hydromagnetic body force, Darcian and Forchheimer drag force terms. The wavy side planes are heated down while the top and vertical planes are thermally insulated. A rectangular heated fin is placed in the lower plane and several different locations of the fin are considered. The transformed, non-dimensional system of coupled non-linear partial differential equations with associated boundary conditions is solved numerically with the Galerkin finite element method (FEM) in the COMSOL Multiphysics software platform. Validation with earlier experimental studies is included. The effects of Darcy number, Hartmann number, volume fraction, undulation number of the wavy wall and Rayleigh number (thermal buoyancy parameter) on the streamlines, isotherms and Bejan number contours are studied in addition to average Nusselt number and average Bejan number. The present simulations have shown that:

(i) With increasing undulation number, there is a slight elevation in average Bejan number at intermediate Rayleigh numbers, whereas the average Nusselt number is substantially boosted, and the effect is maximized at very high Rayleigh number.

(ii) With increasing Hartmann number and Rayleigh number, the average Bejan number is reduced strongly whereas average Nusselt number is only depleted significantly at very high Rayleigh number and high Hartmann number

(iii) With increment in Darcy number (i. e. reduction in permeability of the porous medium layer) there is a substantial elevation in average Nusselt number at high values of Rayleigh number, whereas the contrary response is computed in average Bejan number.

(iv) Effectively stronger magnetic field i. e. Hartmann number, is found to decrease average Nusselt number and also average Bejan number, but only beyond a *critical Rayleigh number* value which is different for each.

(v) With increasing volume fraction, the vortex structures (streamlines) are intensified in particular on the left-hand side of the trapezoidal enclosure whereas the right-hand side vortex is however decelerated owing to momentum conservation and finally splits into two distinct vortex ring structures at very high values of volume fraction.

(vi) Increasing volume fraction also induces significant heating in the enclosure confirming that increasing nanoparticle presence in the hybrid nanofluid achieves the desired thermal enhancement.

(vii)With increasing volume fraction of nanoparticles, Bejan number contour magnitudes are gradually depleted especially near the fin upper surface and sloping walls i. e. they morph from red and yellow contours to blue ones with increasing volume fraction.

The present simulations have revealed some interesting flow characteristics of magnetic nanofluids relevant to hybrid fuel cells and electromagnetic nano-materials processing in cavities. However, the study could be extended to include other metallic nanoparticles e.g. gold/silver nanoparticles [42] and may also address radiative heat transfer [43]. The results of these investigations will be reported imminently.

Acknowledgments

Prof. O. Anwar Bég is grateful to Prof. Rama Gorla of the *Aeronautics and Astronautics Department, US Air Force Institute of Technology, Dayton, Ohio, USA*, for several excellent discussions. He also wishes to express his thanks to his wife, *Khush* for her unwavering support over so many years of advanced research study, and to his many kittens, especially *Milly Dew, Archy, Linda Lu, Barney, Bonnie, Bella* among many others!

References

[1] O. Mahin, E. Bellos, C.N. Markides, R.A. Taylor, A. Alagumalai, L. Yang, C. Qin, B.J. Lee, G. Ahmadi, M.R. Safaei, S. Wongwises. Recent advances in using nanofluids in renewable energy systems and the environmental implications of their uptake. Nano Energy, 2021, 86, 106069. https;//doi.org/10.1016/j.nanoen.2021.106069.

[2] A.G. Olabi, K. Elsaid, E.T. Sayed, S.M. Mahmoud, T. Wilberforce, R.J. Hassiba, M.A. Abdelkareem, Application of nanofluids for enhanced waste heat recovery: A review, Nano Energy, 2021, 84, 105871. https;//doi.org/10.1016/j.nanoen.2021.105871

[3] K. Apmann, R. Fulmer, A. Soto, S. Vafaei. Thermal Conductivity and Viscosity: Review and Optimization of Effects of Nanoparticles. *Materials*. 2021; 14(5):1291. https://doi.org/10.3390/ma14051291

[4] S. Özernic., S. Kakaç, A.G. Yazıcıoğlu, Enhanced thermal conductivity of nanofluids: a state-of-the-art review. Microfluid Nanofluid, 2010, 8, 145–170.

[5] D.M. Samarpan, A. Das. A Short Review of Organic Nanofluids: Preparation, Surfactants, and Applications. Frontiers in Materials 2021, 8,112. https;//doi.org/10.3389/fmats.2021.630182

[6] I. Aliouane, N. Kaid, H. Ameur, H. Laidoudi, Investigation of the flow and thermal fields in square enclosures: Rayleigh-Bénard's instabilities of nanofluids, Thermal Science and Engineering Progress, 10.1016/j.tsep.2021.100959, 25, 100959, 2021. https://doi.org/10.1016/j.tsep.2021.100959.

[7] S.A. Khan, T. Hayat, A. Alsaedi, Irreversibility analysis in Darcy-Forchheimer flow of viscous fluid with Dufour and Soret effects via finite difference method, Case Studies in Thermal Engineering, 26, 101065, 2021. https://doi.org/10.1016/j.csite.2021.101065

[8] X. Xu, S. Chen, C. Chen, C. Xu, C. Wang, Thermal analysis of a novel retarder by using the nanofluid cooling system: Numerical and experimental approaches, Heat Transfer, 50(5), pp. 4127-4143, 2021. https://doi.org/10.1002/htj.22067

[9] C. Zhang, C. Shen, Q. Yang, S. Wei, C. Sun, Blended Ag nanofluids with optimized optical properties to regulate the performance of PV/T systems, Solar Energy, 208, pp. 623-636, 2020. https://doi.org/10.1016/j.solener.2020.08.037

[10] M. Sheikholeslami, Z. Li, M. Shamlooei. Nanofluid MHD natural convection through a porous complex shaped cavity considering thermal radiation. Phys Lett A. 2018, 382, 1615–1632.

[11] A.I. Alsabery, M.A. Sheremet, A.J. Chamkha, I. Hashim. Impact of nonhomogeneous nanofluid model on transient mixed convection in a double lid-driven wavy cavity involving solid circular cylinder. Int J Mech Sci. 2019; 150: 637–655.

[12] I.V. Miroshnichenko, M.A. Sheremet, H.F. Oztop, N. Abu-Hamdeh. Natural convection of alumina-water nanofluid in an open cavity having multiple porous layers. Int J Heat Mass Transf. 2018; 125: 648–657.

[13] A.I. Alsabery, T. Tayebi, A.J. Chamkha, I. Hashim. Effect of rotating solid cylinder on entropy generation and convective heat transfer in a wavy porous cavity heated from below. Int Commun Heat Mass Transf. 2018, 95, 197–209.

[14] H.R. Ashorynejad, A. Shahriari. MHD natural convection of hybrid nanofluid in an open wavy cavity. Results Phys. 2018; 9: 440–455.

[15] Qureshi MZA, Ashraf M. Computational analysis of nanofluids: a review. Eur Phys J Plus. 2018; 133: 1–22

[16] A.I. Alsabery, R. Mohebbi, A.J. Chamkha, I. Hashim I. Effect of local thermal non-equilibrium model on natural convection in a nanofluid-filled wavy-walled porous cavity containing inner solid cylinder. Chem Eng Sci. 2019; 201: 247–263.

[17] S.E. Ahmed, Z.Z. Rashed. MHD natural convection in a heat generating porous medium-filled wavy enclosures using Buongiorno's nanofluid model. Case Stud Therm Eng. 2019; 14: 100430

[18] A.E. Moghadam, A.J. Moghadam. Optimal design of geometrical parameters and flow characteristics for Al_2O_3/water nanofluid inside corrugated heat exchangers by using entropy generation minimization and genetic algorithm methods. Appl Therm Eng. 2019; 149: 889–898

[19] S. Salman, A.R. Abu Talib, S. Saadon, M.T. Hameed Sultan, Hybrid nanofluid flow and heat transfer over backward and forward steps: A review, Powder Technology, 363 (1), 448-472, 2020.

[20] S. Suresh, K.P. Venkitaraj, P. Selvakumar, M. Chandrasekar, Effect of Al_2O_3-Cu/water hybrid nanofluid in heat transfer, Experimental Thermal and Fluid Science, 38, 54-60, 2012.

[21] A. Shahsavar, S.P. Talebizadeh, D. Toghraie, Free convection heat transfer and entropy generation analysis of water-Fe3O4/CNT hybrid nanofluid in a concentric annulus, International Journal of Numerical Methods for Heat & Fluid Flow, 29(3), 915-93, 2019.

[22] M.N. Labib, M.J. Nine, H. Afrianto, H. Chung, H. Jeong, Numerical Investigation on effect of base fluids and hybrid nanofluid in forced convective heat transfer, International Journal of Thermal Sciences, 71, 163-171, 2013.

[23] A. Shenoy, M. Sheremet, I. Pop. Convective flow and heat transfer from wavy surfaces: viscous fluids, porous media and nanofluids. Boca Raton: CRC Press, Florida, USA, 2016.

[24] M.M. Ali, R. Akhter, M.A. Alim, Hydromagnetic natural convection in a wavy-walled enclosure equipped with hybrid nanofluid and heat generating cylinder, Alexandria Engineering Journal, 60(6), 5245-5264, 2021.

[25] F.M. Azizul, A.I. Alsabery, I. Hashim, A.J. Chamkha, Impact of heat source on combined convection flow inside wavy-walled cavity filled with nanofluids via heat line concept, Applied Mathematics and Computation, 393, 125754, 2021. https://doi.org/10.1016/j.amc.2020.125754

[26] M.S. Ishak, A.I. Alsabery, I. Hashim, A.J. Chamkha, Entropy production and mixed convection within trapezoidal cavity having nanofluids and localized solid cylinder, Scientific Reports, 11, 14700, 2021. https://doi.org/10.1038/s41598-021-94238-w

[27] S.E. Ahmed, Z.Z. Rashed, MHD natural convection in a heat generating porous medium-filled wavy enclosures using Buongiorno's nanofluid model, Case studies in Thermal Engineering, 14, 100430, 2019. https://doi.org/1016/j.csite.2019.100430.

[28] D. Tripathi, R. Jhorar, O. Anwar Bég and A. Kadir, Electro-magneto-hydrodynamic peristaltic pumping of couple stress biofluids through a complex wavy micro-channel, *J. Molecular Liquids,* 236, 358-367 (2017).

[29] O. Anwar Bég, S.S. Motsa, T. A. Bég, A. Kadir, A.J. Abbas and A. Sohail, Numerical study of nonlinear heat transfer from a wavy surface to a high permeability medium with pseudo-spectral and smoothed particle methods, *Int. J. Applied Computational Mathematics,* 3, 3593–3613 (2017).

[30] M.J. Uddin, W.A. Khan, and O. Anwar Bég, Bioconvection nanofluid slip flow past a wavy surface with applications in nano-biofuel cells *Chin. J. Physics,* 55, 2048-2063 (2017).

[31] Latifa M.Al-Balushi, M. Uddin and M.M.Rahman, Natural convective heat transfer in a square enclosure utilizing magnetic nanoparticles, *Propulsion and Power Research, 8 (3)* 194-209 (2019).

[32] M.M. Rahman, M.S. Alam, N. Al-Salti, I.A. Eltayeb, Hydromagnetic natural convective heat transfer flow in an isosceles triangular cavity filled with nanofluid using two-component nonhomogeneous model, *Int. J. Therm. Sci*. 107 (2016) 272-288.

[33] O. Anwar Bég, K. Venkatadri, V.R. Prasad, Tasveer A. Bég, Henry J. Leonard, MAC computation of magnetohydrodynamic convection flow in a non-Darcian porous enclosure saturated with electrically conducting Helium, *Proc. IMechE-Part C – J. Mechanical Engineering Science (2021). 21 pages. DOI: 10.1177/09544062211003624*

[34] V. K. Narla, Dharmendra Tripathi and O. Anwar Bég, Analysis of entropy generation in biomimetic electro-osmotic nanofluid pumping through a curved channel with Joule dissipation, *Thermal Science and Engineering Progress (2019). doi.org/10.1016/j.tsep.2019.100424 (15 pages)*

[35] H. Thameem Basha, R. Sivaraj, V. R. Prasad, O. Anwar Bég, Entropy generation of tangent hyperbolic nanofluid flow over a circular cylinder in the presence of nonlinear Boussinesq approximation: A non-similar solution, *J. Thermal Analysis and Calorimetry (2020).* https://doi.org/10.1007/s10973-020-09981-5

[36] B. Vasu, R.S.R. Gorla, P. V. S. N. Murthy and O. Anwar Bég, Entropy analysis on convective film flow of power-law fluid with nanoparticles along an inclined plate, *J. Applied Mechanics and Technical Physics*, 60, 5, 1-15 (2019).

[37] B. Mallikarjuna, G. Gopi Krishna, J. Srinivas and O. Anwar Bég and Ali Kadir, Spectral numerical study of entropy generation in magneto-convective viscoelastic flow through a

deformable porous medium with thermal radiation and buoyancy effects, *ASME J. Thermal Science and Engineering Applications*, 14, 011008-1 to 12 (2022).

[38] M. Norouzi, S. Dorrani, H. Shokri and O. Anwar Bég, CFD (COMSOL) simulation of viscous dissipation effects on miscible thermo-viscous fingering instability in porous media, *Int. J. Heat Mass Transfer*, 129, 212-223 (2019).

[39] COMSOL Modeling Software, *COMSOL.com*. Comsol, Inc. (2015).

[40] Krane R, Jesee J. Some detailed field measurement for a natural convection flow in a vertical square enclosure. In: *Proceedings of the 1st ASME-JSME Thermal Engineering Joint Conference, Honolulu, March 20-24*, 1983, pp. 323-329.

[41] Cramer, K.C. and Pai, S.I., *Magnetofluid Dynamics for Engineers and Applied Physicists*, MacGraw-Hill, New York, USA (1973).

[42] Sireetorn Kuharat, O. Anwar Bég, Ali Kadir, B. Vasu, Tasveer A. Bég and W.S. Jouri, Computation of gold-water nanofluid natural convection in a three-dimensional tilted prismatic solar enclosure with aspect ratio and volume fraction effects, *Nanoscience and Technology- An International Journal, 11(2):141–167 (2020).*

[43] S. Kuharat, O. Anwar Bég, Ali Kadir and B. Vasu, Computation of metallic nanofluid natural convection in a two-dimensional solar enclosure with radiative heat transfer, aspect ratio and volume fraction effects, *Arabian J. Science and Engineering (2020). (19 pages). doi.org/10.1007/s13369-020-04678-1*